The Effect of Spin−Orbit Splitting on the Association Kinetics of Barrierless Halogen Atom−Hydrocarbon Radical Reactions

Ahren W. Jasper*

Combustion Research Facility, Sandia National Laboratories, P.O. Box 969, Livermore, California 94551-0969

Stephen J. Klippenstein and Lawrence B. Harding

Chemical Sciences and Engineering Division, Argonne National Laboratory, Argonne, Illinois 60439

Received: February 18, 2010; Revised Manuscript Received: March 25, 2010

The effect of the geometry dependence of spin−orbit splitting on transition state theory (TST) predictions for radical−radical recombination rate coefficients is examined. The effects are illustrated with direct ab initio variable-reaction-coordinate (VRC)-TST calculations for the reactions of two types of hydrocarbon radicals (R = CH_3 and CH_2CHCH_2) with three halogen atoms (X = F, Cl, and Br). These halogen atoms exhibit a range of spin−orbit interaction strengths, while their interactions with the two hydrocarbon radicals exhibit a range of attractiveness. The transition state dividing surfaces for these barrierless reactions occur over a range of R−X fragment separations (∼3−7 Å) where the magnitude of the spin−orbit splitting is strongly geometry dependent. Perturbative models for incorporating the energetic effect of spin−orbit splitting into barrierless kinetics are presented and tested. Simply neglecting the variation in the spin−orbit splitting is demonstrated to contribute an error of less than 15% to the predicted rate coefficients for all but the CH_2CHCH_2 + Br reaction, where its neglect increases the rate by up to a factor of 2. For the CH_2CHCH_2 + Br reaction, the effect of spin−orbit splitting is not perturbative and instead qualitatively changes the long-range interaction potential and association dynamics. The present theoretical predictions are compared with available experimental measurements and previous theoretical work. For the CH_3 + F association reaction, the errors associated with limitations in the basis set and in the active space are studied, and a detailed comparison is made between VRC-TST and rigid rotor-harmonic oscillator variational TST.

I. Introduction

During molecular bond formation between a radical with degenerate electronic states (such as a halogen atom) and some other radical or molecule, the spin−orbit splitting associated with the degenerate radical generally decreases to near zero. The kinetic significance of this variation in the spin−orbit interaction depends on the magnitude of this variation relative to the magnitude of the interaction potential in the transition state region (and also relative to thermal energies). Theoretical predictions for the recombination rate coefficient typically consider one of two limits to account for this spin−orbit splitting. If the transition state lies at very large fragment separations, then the spin−orbit splitting is presumed to be close to its asymptotic fragment value, and its variation is ignored. Alternatively, in the opposite limit of a small fragment separation at the transition state, the spin−orbit splitting is presumed to be small enough that its effect on the potential in the transition state region may be ignored.

The appropriateness of these two pictures and the kinetic significance of the variation depends on the details of the two interactions. At temperatures that greatly exceed the asymptotic spin−orbit interaction energy, the two limiting pictures yield the same predictions for the rate coefficients. However, at lower temperatures, the effect may be quite substantial with the two limits yielding very different predictions. Unfortunately, it is not clear which limit should be more generally appropriate.

To date there have been very few studies of this variation and its effect on the association kinetics. Tashiro and Schinke employed time-dependent wave packets to study the capture rate for O + O_2 on multiple electronic states and found little effect from spin−orbit coupling.[1] The qualitative analysis in our transition state theory (TST) study of the CH_3 + Cl reaction suggested that the predictions for the capture rate coefficient are strongly dependent on this variation in the spin−orbit interaction strength.[2] For the CH_3 + OH reaction, our TST analysis, which included a geometry dependent spin−orbit interaction, found that the simple neglect of the variation yielded accurate predictions for the capture rate.[3]

In this article, we consider the balance between the variation in the spin−orbit interaction and the strength of the chemical interaction for six representative reactions. In particular, we consider the association reactions of methyl (CH_3) and allyl (CH_2CHCH_2) radicals with the three halogens F, Cl, and Br. The consideration of three halogen atoms and two hydrocarbon radicals (one of which is resonantly stabilized) allows us to determine the effect of the spin−orbit splitting on the rate coefficients for a wide range of spin−orbit coupling strengths (∼400 to 4000 cm^{-1}) and dynamical regimes. The methyl radical represents a prototypical hydrocarbon radical, while the resonance stabilization in the allyl radical yields transition states that are relatively tight for a barrierless recombination.

The dynamical bottlenecks for barrierless association typically occur at fragment separations that are large relative to chemical bonding distances, and these separations vary significantly as a function of energy and temperature. The theoretical determi-

* To whom correspondence should be addressed. E-mail: ajasper@sandia.gov.

10.1021/jp1015092

nation of the kinetics of such radical−radical reactions is complicated by the need to characterize the wide region of the interaction potential energy surface associated with these dynamical bottlenecks. Here, the kinetics for these six reactions are studied with variable reaction coordinate transition state theory[4−6] (VRC-TST), which has been developed to accurately and efficiently treat such barrierless reactions. VRC-TST, coupled with direct evaluations of the interaction potential energy surface using multireference electronic structure theory methods, has recently been used to predict accurate rate coefficients for several radical−radical hydrocarbon association reactions[7−10] and for reactions involving oxygen-containing species.[3,11] This direct coupling with electronic structure evaluations allows for the explicit inclusion of the geometry dependent spin−orbit interaction in the TST analysis. Here, we test the importance of explicitly considering this geometry dependence of the spin−orbit splitting over the extended region of the potential energy surface in VRC-TST calculations.

The reactions of halogen atoms with hydrocarbon radicals are also of chemical interest. Chlorine and bromine in the atmosphere deplete ozone, and long-lived halogen source gases (CFCs, halons, etc.) play an important role in delivering chemically active halogen atoms to the stratosphere.[12] Despite considerable attention, significant uncertainties in the atmospheric chemistry of halocarbons remain. Accurate laboratory measurements of the rate coefficients of reactions involving radicals are often difficult to achieve because of their short lifetimes, and fast competing reactions may lead to complex secondary chemistries. Thus, another goal of the present study is to validate the ab initio VRC-TST method for predicting rate coefficients for barrierless reactions involving halogen atoms.

Accurate rate coefficients for the $CH_3 + X$ (X = F, Cl, and Br) reactions are of practical importance in laboratory measurements of rate coefficients for the atmospherically relevant $CH_4 + X \rightarrow CH_3 + HX$ reactions, as the reaction of the free halogen atom with the methyl radical product may comprise an important secondary pathway for radical consumption. There are relatively few experimental and theoretical studies of the $CH_3 + X$ association reactions in the literature. Biederhase et al.[13] measured the rate coefficient for $CH_3 + F$ at room temperature, and Wang et al.[14] characterized the energetics and kinetics of the CH_3F system in detail theoretically. Krasnoperov et al.[15] measured the rate coefficient for $CH_3 + Br$ at room temperature and elevated pressures. The $CH_3 + Cl$ reaction was studied[2] both theoretically and experimentally at low pressures, and, although good agreement between theory and experiment was obtained, some ambiguity in the treatment of the spin−orbit splitting associated with the Cl atom was identified in the predicted high-pressure rate coefficient.

The reactions of F, Cl, and Br with the resonantly stabilized allyl radical ($\bullet CH_2-CH=CH_2$) are even less studied. Bedjanian et al.[16] measured the room temperature rate for $CH_2CHCH_2 +$ Br association. Harding et al.[9] previously studied the reactions of several resonantly stabilized radicals, including allyl, with H atoms using the ab initio VRC-TST method, and good agreement between the predicted rates and available experimental values was obtained in that study. The VRC-TST dynamical bottlenecks (transition states) for association in reactions involving resonantly stabilized radicals and H atoms were shown to occur at short fragment distances relative to those for other radical−radical addition reactions, such as $CH_3 + H$.

II. Theory

High pressure limit (capture) rate coefficients for six R + X reactions (R = CH_3, CH_2CHCH_2; X = F, Cl, Br) were computed using direct ab initio VRC-TST, as implemented in the computer code VaReCoF[17] and as described in detail elsewhere.[6] A dynamical correction of 0.9 was applied to correct for recrossing, as determined previously for atom-molecule reactions.[7]

Two types of transition state dividing surfaces were considered: center of mass (CoM) dividing surfaces with fixed CoM separations varying from 2 to 7 Å and multifaceted (MF) dividing surfaces[18] with a pair of pivot points displaced from the radical C atom above and below the plane of the hydrocarbon fragment. MF dividing surfaces are generalizations of VRC[4] dividing surfaces and are often necessary for accurately treating barrierless association reactions with multiple reactive sites at moderate and high temperatures.

Thermal rate coefficients were obtained via Boltzmann averages over variationally optimized microcanoncal rates $k(E,J)$, where E is the total energy and J is the total angular momentum. We also consider canonical variational theory (CVT) calculations, where the variational optimizations were carried out at the thermally resolved level. The CVT rate coefficients are upper limits to the more accurate microcanonical ones and are not emphasized. The CVT calculations are useful for simplifying the interpretation of the kinetics calculations, however, because (for each temperature) a single dividing surface can be identified as the dynamical bottleneck. Specifically, we report the distance of the forming C-X bond at the minimum-energy point on the CVT dividing surface for each temperature T, which is labeled $R^*_{CVT}(T)$.

For the $CH_3 + X$ reactions, several MF dividing surfaces were tested and found to not contribute significantly to the microcanonical variational optimizations over the temperature range considered here (300−2500 K), lowering the predicted thermal rate coefficients by no more than 2%. Although MF dividing surfaces associated with pivot points displaced from the CoM of the methyl radical were found to be important in characterizing the kinetics of the $CH_3 + H$,[7] $CH_3 + CH_2$,[11] and $CH_3 + CH_3$[8] association reactions, they were not required for the $CH_3 + OH$[3] reaction. The heavier and less-bulky fragments and longer-ranged interaction potentials for the OH and X partners reduces the importance of the shape of the methyl radical in determining the association kinetics for these reactions.

For the $CH_2CHCH_2 + F$ reaction, MF dividing surfaces with various pivot point distances and orientations were considered, and the inclusion of these MF dividing surfaces lowered the rate coefficient by less than 3%. MF dividing surfaces were not considered for the $CH_2CHCH_2 + Cl$ and Br reactions.

The interaction potential energy surfaces were evaluated directly during the VRC-TST calculations using multireference perturbation theory[19] (CASPT2) and the augmented Dunning family of basis sets.[20,21] The aug-cc-pVDZ-PP pseudopotential[22] was used to represent the filled 1s, 2s, and 2p orbitals of Br; otherwise, all electrons were treated explicitly using the aug-cc-pVDZ basis set for the methyl reactions and the aug′-cc-pVDZ basis set[23] for the allyl reactions. The prime on the prefix "aug" denotes that diffuse basis functions were not included for the H atoms. The CH_3 and CH_2CHCH_2 fragments were kept fixed at their B3LYP/6-311++G(d,p) geometries.

The CASPT2 active space consisted of six electrons in four orbitals (6e,4o) for the $CH_3 + X$ reactions, corresponding at large fragment separations to the radical orbital of CH_3 and the three equivalent valence p orbitals of the halogen atom. Additional calculations were carried out along the minimum energy path for $CH_3 + F$ association using a full valence (FV) (14e,11o) active space and using larger basis sets. For the $CH_2CHCH_2 + X$ reactions, the three π orbitals on the allyl

radical and the three p orbitals on the halogen atom were included in the active space, i.e., a (8e,6o) active space was used. Orbitals were optimized for the average energy of the three lowest singlet states during the CASSCF step of the CASPT2 calculation to avoid root flipping problems at extended fragment separations.

Spin−orbit splitting in the VRC-TST rate calculations was computed using the CASSCF method, the Breit-Pauli Hamiltonian,[24] the active spaces discussed above, and the cc-pVTZ basis set. This method predicts spin−orbit splittings E_{SO} for the isolated F, Cl, and Br atoms of 390, 820, and 3517 cm^{-1}, respectively, which may be compared with the experimental values of 404, 881, and 3685 cm^{-1}.[25] For the allyl radical calculations, the cc-pVDZ basis set was used to evaluate the spin−orbit splitting; this method predicts atomic spin−orbit splittings of 374, 818, and 3510 cm^{-1} for F, Cl, and Br, respectively. The accuracy of this theoretical treatment of the spin−orbit splitting is consistent with a previous, more extensive evaluation of these methods,[26] where the predicted splittings were shown to be only weakly dependent on the level of electron correlation and basis set.

In the VRC-TST calculations, the vibrational, rotational, and electronic partition functions are treated as separable, and the electronic partition function of the reactants is given by

$$Q_e(T) = 2(4 + 2\exp(-E_{SO}/kT)) \quad (1)$$

III. Results and Discussion

III.A. The Geometry Dependence of Spin−Orbit Splitting. The triply degenerate nonrelativistic ^2P ground state of a halogen atom X is split by spin−orbit interactions into a $^2P_{3/2}$ state (which is stabilized by $E_{SO}/3$ relative to the ^2P state) and a $^2P_{1/2}$ state (which is destabilized by $2E_{SO}/3$). The interaction with a hydrocarbon radical R further splits the degeneracies. With spin−orbit interactions neglected, the R + X asymptote correlates with one attractive singlet surface, two repulsive singlet surfaces, and three repulsive triplet surfaces. Spin−orbit interactions mix these surfaces into one attractive surface and 11 repulsive surfaces. In the present work, the R + X reactions are assumed to occur exclusively on the ground state surface, and dynamical non-Born−Oppenheimer effects, such as transitions between the coupled electronic states, are not considered.

Figure 1 shows the spin−orbit stabilization ε_{SO} of the ground state surface scaled by its maximum value $E_{SO}/3$ along the minimum energy paths for association for the six reactions considered here. In the R + X asymptote, ε_{SO} is equal to the atomic stabilization energy; ε_{SO} decreases as the R−X complex is formed and is generally small for the RX molecule. The calculated spin−orbit stabilization is similar for the methyl and allyl fragments, is strongly dependent on the forming C−X distance (R_{CX}) for R_{CX} = 3−5 Å, and is relatively independent of the orientation of the methyl and allyl fragments for attractive orientations.

Figure 1 also shows the C−X distances associated with the minimum-energy geometries on the CVT dividing surfaces (R^*_{CVT}) computed using the VRC-TST method. A detailed discussion of the results of the VRC-TST calculations is given in sections III.B and III.C. For now, we simply note that R^*_{CVT} ≈ 3−6 Å, which includes the range of C−X distances where the spin−orbit splitting is strongly geometry dependent.

The interaction energies including spin−orbit splitting V_{SO} along the minimum energy paths for association are shown in Figure 2. As expected, the interaction potentials are shorter

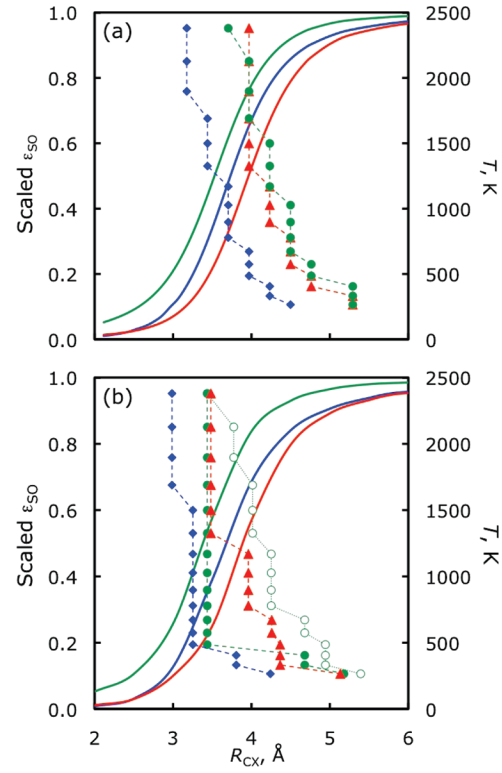

Figure 1. The left axis shows the scaled spin−orbit stabilization energies ε_{SO} (solid lines) along the (a) CH_3 + X and (b) CH_2CHCH_2 + X minimum energy paths for association for X = F (blue), Cl (red), and Br (green). Also shown is R^*_{CVT} (filled symbols; diamonds for F, triangles for Cl, and circles for Br) as a function of temperature (right axis). For the CH_2CHCH_2 + Br reaction, the values of R^*_{CVT} for the c-SO calculation are also shown as open symbols.

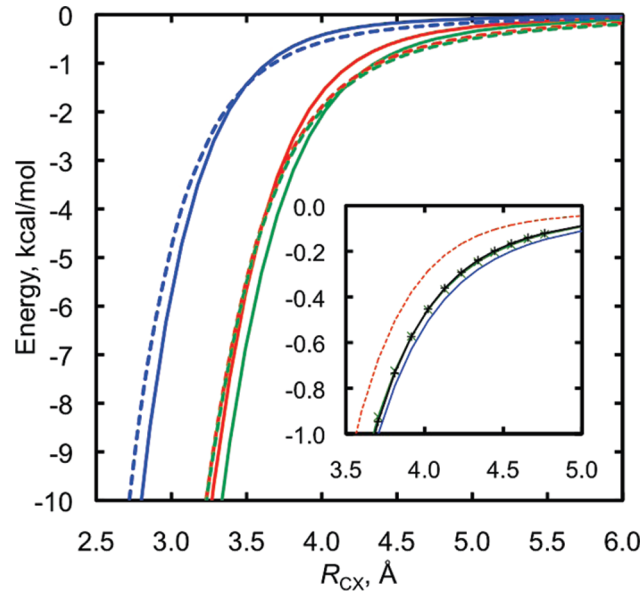

Figure 2. CASPT2/aug-cc-pVDZ interaction energies V_{SO} for the CH_3 + X (solid) and CH_2CHCH_2 + X (dashed) reactions along the minimum energy paths for association for X = F (blue), Cl (red), and Br (green). The inset reproduces the CH_3 + F energy and shows the effect of using the cc-pVDZ basis (red dotted), extrapolating to the CBS limit (green X), and using a full valence (FV) active space (black +); the CBS and FV curves are nearly coincident on this scale.

ranged for the smaller halogen F and are similar for Cl and Br, which have similar atomic radii.[27] The allyl radical interaction potentials are somewhat less attractive than those for the methyl radical reactions at short fragment separations due to the

increased stability of the allyl radical arising from resonance stabilization. The long-range potentials for the allyl reactions are more attractive, however, as the larger allyl radicals feature stronger dispersion interactions. These differences suggest that the transition states for the allyl reactions at moderate and high temperatures should occur at shorter separations than for the methyl reactions, which is in fact the case (cf. Figure 1).

Before we discuss the effect of the geometry dependence of the spin−orbit splitting on the predicted barrierless kinetics, we first consider the simpler case of incorporating spin−orbit splitting into TST calculations for reactions with a barrier, such as $CH_4 + X \rightarrow CH_3 + HX$. For reactions with a barrier, the saddle point is typically located at bond distances only moderately extended relative to chemical distances, and the dynamically important region of the potential energy surface is often fairly localized around the saddle point. To incorporate the energetic effect of spin−orbit splitting, it is often a good approximation to neglect the geometry dependence of the spin−orbit splitting near the barrier and to simply adjust the nonrelativistic barrier upward by $E_{SO}/3$. The relative kinetic effect of such an adjustment is

$$k'_{SO} = k \exp(-E_{SO}/3k_BT) \quad (2)$$

where k and k'_{SO} are the nonrelativistic and corrected thermal rate coefficients, respectively.

The dynamical information in Figure 1 indicates that the accuracy of the simple thermal correction in eq 2 is questionable for barrierless reactions. First, the magnitude of the spin−orbit splitting varies from ∼10−90% of its asymptotic value over the kinetically relevant region of the potential energy surface. For barrierless reactions, it may therefore be more appropriate to correct the nonrelativistic rate using

$$k''_{SO} = k \exp(-CE_{SO}/3k_BT) \quad (3)$$

where $C \approx 0.1-0.9$ and is a function of temperature. Second, the magnitude of the spin−orbit splitting can be similar to that of the interaction energy (shown in Figure 2) in the long-range region of the potential energy surface. Therefore, the kinetic effect of spin−orbit splitting may not be perturbative, as the treatments in eqs 2 and 3 imply. Instead, spin−orbit splitting may qualitatively change the nature of the long-range reactive surface and the geometries associated with the dynamical bottlenecks for barrierless association.

In general, spin−orbit splitting increases the energy of the reactive surface relative to the reactants and consequently reduces the predicted rate. The quantitative effect of spin−orbit splitting on barrierless kinetics depends sensitively on the magnitude of the splitting relative to the magnitude of the interaction energy at the variationally optimized dynamical bottlenecks for association.

To aid in the interpretation of the theoretical results presented in the rest of this section, we define

$$\Delta(R_{CX}) = (V - V_{SO})/V_{SO} \quad (4)$$

where V_{SO} and V are the R + X interaction energies with and without the geometry dependence of the spin−orbit splitting explicitly included at some distance R_{CX} along the minimum energy path for association. Equation 4 is therefore the relative change in the interaction energy when the geometry dependence of the spin−orbit splitting is neglected.

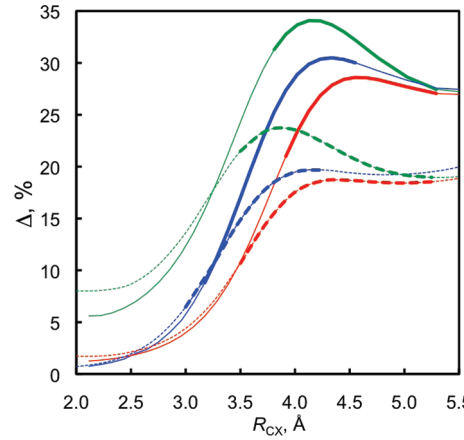

Figure 3. Relative change in the interaction energy due to the neglect of the geometry dependence of spin−orbit splitting (Δ in eq 4) for the CH_3 + X (solid) and CH_2CHCH_2 + X (dashed) reactions along the minimum energy paths for association for X = F (blue), Cl (red), and Br (green). The thick lines highlight the range of R^*_{CVT} for 300−2500 K for each reaction.

TABLE 1: VRC-TST Capture Rate Coefficients k_{SO}[a]

reaction	A (cm^3 molecule^{-1} s^{-1})	n	E (K)
CH_3 + F	5.96×10^{-11}	0.0682	−5.42
CH_3 + Cl	9.25×10^{-11}	0.0501	18.7
CH_3 + Br	9.01×10^{-11}	0.124	8.03
CH_2CHCH_2 + F	7.16×10^{-11}	0.0671	−1.28
CH_2CHCH_2 + Cl	1.00×10^{-10}	0.0117	23.2
CH_2CHCH_2 + Br	6.13×10^{-11}	−0.0587	−16.8

[a] Fit to $k_{SO} = A\ (T/298\ \text{K})^n \exp(-E/T)$ for T = 300−2500 K.

Figure 3 shows Δ for the six R + X reactions. In general, Δ is largest for Br, which has the largest spin−orbit splitting. For Cl, Δ is reduced relative to Br as V_{SO} is similar for Br and Cl, but the spin−orbit splitting for Cl is considerably smaller. The spin−orbit splitting for F is even smaller, but the weaker interaction potential results in values for Δ that are larger than those for Cl.

As seen in Figure 1, the spin−orbit splitting along the reaction path is similar for the allyl and methyl reactions, and Δ differs for the two hydrocarbon radicals primarily due to differences in V. At short separations, Δ is somewhat larger for the allyl radical than for the methyl radical due to the weaker interactions, although the effect is small. At larger fragment separations, Δ is considerably reduced for the allyl + X reactions relative to the methyl + X reactions due to the more attractive long-range interaction potentials for the allyl radicals, as discussed above.

Figure 3 suggests that the kinetic effect of spin−orbit splitting will be somewhat larger for the methyl reactions and will be similar for the three halogen atoms.

III.B. Methyl Radical−Halogen Atom Reactions. In this section and section III.C, rate coefficients are reported for the methyl radical−halogen atom and allyl radical−halogen atom reactions. Our best estimates for each rate coefficient k_{SO} were obtained by treating spin−orbit splitting as explicitly geometry dependent over the three-dimensional interaction potential during the direct VRC-TST calculations. These rate coefficients were fit to modified Arrhenius forms and are summarized in Table 1.

As discussed in section II, microcanonical variational optimizations were used to compute the VRC-TST rate coefficients reported here. The use of CVT optimizations resulted in rate

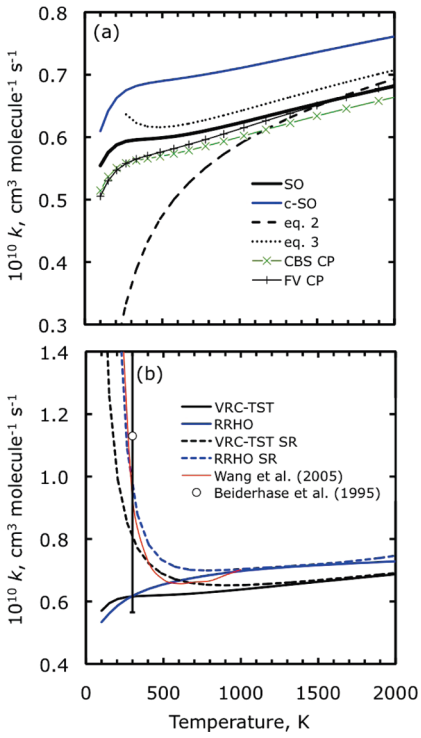

Figure 4. (a) VRC-TST CH_3 + F capture rate coefficient k_{SO} (solid black). Also shown are the rate coefficients calculated assuming a constant spin−orbit interaction k^c_{SO} (solid blue), correcting k^c_{SO} using eqs 2 (dashed black) and 3 (dotted black), and using one-dimensional correction potentials (CP) to approximate the complete basis set (CBS) limit (green X) and an FV active space (black +). (b) VRC-TST (black) and RRHO (blue) rate coefficients. Short range (SR) calculations with restricted sets of dividing surfaces for both methods are shown as dashed lines. The previous theoretical result of Wang et al.[14] is shown in red, and the experimental result of Beiderhase et al.[13] at 300 K is indicated by a circle.

coefficients that are 10−40% larger than the microcanonical rate coefficients for 300−2500 K, with larger errors at low temperatures and for the allyl + Br reaction.

VRC-TST capture rate coefficients were also calculated with the geometry dependence of the spin−orbit splitting neglected, and the error associated with this simplifying approximation will be discussed. Because the interaction energy is evaluated relative to the reactants in the VRC-TST calculations, assuming a constant spin−orbit splitting equal to its asymptotic value is kinetically equivalent to neglecting the effect of the spin−orbit splitting entirely (as in a calculation using a nonrelativistic potential). We label rate coefficients calculated using this approximation k^c_{SO}, where "c" denotes a constant (geometry-independent) spin−orbit splitting, and we note that k^c_{SO} is equal to the nonrelativistic rate k.

CH_3 + F. VRC-TST rate coefficients for CH_3 + F association for several treatments of spin−orbit splitting are shown in Figure 4a. The kinetic effect of explicitly considering the geometry dependence of spin−orbit splitting may be quantified by comparing k_{SO} with k^c_{SO}, where the use of a constant spin−orbit splitting artificially increases the predicted rate by only 10−13%. As seen in Figure 1, R^*_{CVT} = 3.2−4.5 Å for 300−2500 K, and the spin−orbit splitting varies from 0.9 to 0.2 of its asymptotic value over this dynamically important region of the potential energy surface. (Note that, because the microcanonical variational optimizations were used to calculate k_{SO}, the kinetically relevant region of the potential energy surface is somewhat broader than the region indicated by R^*_{CVT}.) The small magnitude of the spin−orbit splitting for F corresponds to relative changes in the interaction potential Δ of only 9−30% for R_{CF} = 3.2−4.5 Å (cf. Figure 3), which is similar but somewhat greater than the magnitude of the observed kinetic effect.

The use of eq 2 to correct the nonrelativistic rate results in a significant error at room temperature (40%) and a qualitatively incorrect temperature dependence, as seen in Figure 4a. Clearly, the use of the atomic spin−orbit energy correction in eq 2 overcorrects the nonrelativistic rate at low temperatures. A more useful correction for barrierless reactions is given by eq 3, and such an approach is practical so long as $C(T)$ can be reliably estimated. Figure 4a shows the improved result of applying eq 3, where

$$C(T) = 1 - \frac{\varepsilon_{SO}(R^*_{CVT}(T))}{E_{SO}/3} \qquad (5)$$

which can be readily obtained from the results of the VRC-TST calculations and the spin−orbit splittings along the reaction path shown in Figure 1. The success of eqs 3 and 5 suggests that spin−orbit effects are perturbative for the CH_3 + F reaction, but that corrections less than the maximum asymptotic correction (as in eq 2) are required for accurate barrierless kinetics.

Next, we compare the error identified with the neglect of the geometry dependence of the spin−orbit splitting with other sources of error present in the evaluation of the interaction potential, namely, the use of finite basis sets and limited active spaces. To evaluate the basis set sensitivity of the predicted rate coefficient, the CH_3 + F interaction energy was computed along the minimum energy path for association for the cc-pVDZ, aug-cc-pVDZ, aug-cc-pVTZ, and aug-cc-pVQZ basis sets and the (6e,4o) active space. The complete basis set (CBS) limit[28] was estimated from aug-cc-pVTZ and aug-cc-pVQZ calculations. The results are shown in the inset of Figure 2. The CBS interaction energy is less attractive than the aug-cc-pVDZ interaction energy along the minimum energy path by 3−10% for R_{CF} = 3.2−4.5 Å. The cc-pVDZ interaction energy is significantly less attractive than the aug-cc-pVDZ interaction energy (by 60−20% for R_{CF} = 3.2−4.5 Å). A contour plot of the CH_3 + F interaction potential in a plane perpendicular to the methyl radical is shown in Figure 5a for the CASPT2/aug-cc-pVTZ method. As shown in Figure 5b, the aug-cc-pVTZ and aug-cc-pVDZ basis sets predict very similar interaction energies, whereas the interaction energy for the cc-pVDZ basis set is again much less attractive (cf. Figure 5c).

The less attractive cc-pVDZ surface suggests that it will significantly underestimate the rate. We find, however, that the VRC-TST rate coefficient computed using the cc-pVDZ basis set is lower than the aug-cc-pVDZ result by only ∼5%. This result is due to the presence of spurious wells in the cc-pVDZ surface (as seen in Figure 5c at Y = 0 and Z = ±7 au), resulting in a cancellation of errors in the computed rate coefficients, as was observed for the isoelectronic CH_3 + OH reaction.[3] The cc-pVDZ basis set is not considered further.

The sensitivity of the predicted results to the choice of active space in the CASPT2 calculations was also considered. Using an FV active space (14e,11o) and the aug-cc-pVDZ basis set, the interaction energy along the minimum energy path differs from the minimal active space (6e,4o) result by −4 to 20% for R_{CF} = 3−4.5 Å, as shown in Figure 2.

Taken together, errors in the interaction energy resulting from the use of an incomplete basis set and a limited active space may be expected to have a combined upper limit of ∼30%,

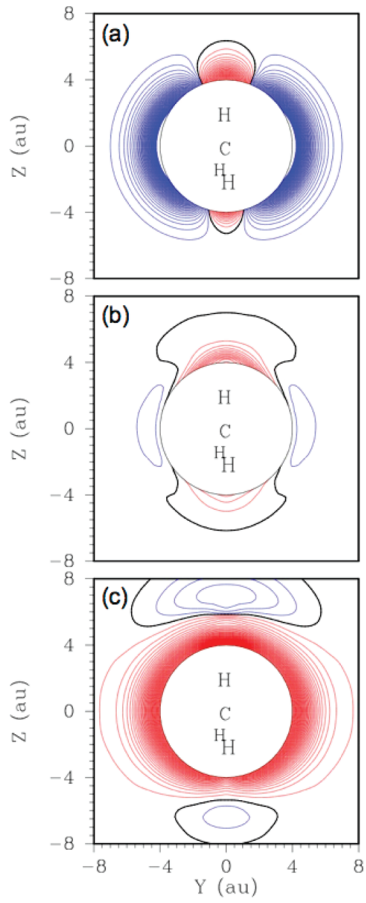

Figure 5. (a) Two-dimensional contour plot of the CASPT2/aug-cc-pVTZ CH_3 + F interaction potential in a plane perpendicular to the methyl radical. Difference potentials for the (b) CASPT2/aug-cc-pVDZ and (c) CASPT2/cc-pVDZ methods relative to CASPT2/aug-cc-pVTZ are also shown. The blue contours are negative, the red contours are positive, and the black line is the zero contour. The contour spacing is 1 kcal/mol for (a) and 0.2 kcal/mol for panels b and c. 1 au = 0.529 Å.

and in both cases the higher level treatments typically act to make the relative potential less attractive and thereby decrease the predicted rate coefficient. We estimated the effect of these errors on the VRC-TST rate coefficient using a one-dimensional correction potential scheme, as employed elsewhere.[7,8] Briefly, energies along the minimum energy path for association were used to define one-dimensional CBS and FV active space correction potentials, which were then used to correct VRC-TST calculations carried out with a full-dimensional (6e,4o) CASPT2/aug-cc-pVDZ potential energy surface. This scheme assumes that the energetic effect of the increased basis set and larger active space is insensitive to the orientation of the reacting fragments.

We find that the CBS correction potential lowers the predicted rate coefficient by only 2−6% for 300−2500 K, and the FV correction potential lowers the predicted rate coefficient by 6% at room temperature and increases the rate coefficient by 1% at 2500 K, as shown in Figure 4a.

This analysis suggests that the CASPT2/aug-cc-pVDZ method with the (6e,4o) active space is sufficiently accurate for the CH_3 + F system. Furthermore, neglecting the geometry dependence of the spin−orbit splitting is the largest of the three sources of error considered here. That is, estimates of the finite basis set error, limited active space error, and spin−orbit geometry dependence error in the rate calculations are 2−6%, 1−6%, and 10−13%, respectively. The uncertainties in the predicted rates are roughly 1/2 the relative changes in the interaction energies due to these effects.

The experimental measurement of Beiderhase et al.[13] for the overall rate coefficient at room temperature is a factor of 2 larger than the present prediction, but is in excellent agreement with ref 14. Note, however, that the experimental measurement was fairly indirect and was assigned an uncertainty of a factor of 2. It is also worth noting that the experimental measurement is really for the total rate coefficient and so some portion of the apparent discrepancy between experiment and the present predictions may be due to a contribution from a triplet abstraction channel. This abstraction channel has a saddle point that is very close to thermoneutral, and the calculations of Wang et al.[14] suggest that the rate coefficient for this channel is $\sim 1 \times 10^{-11}$ cm^3 molecule^{-1} s^{-1} at room temperature. For completeness, we have also predicted the rate coefficient for this channel employing conventional TST (but with higher level energy estimates), obtaining a value of 2.5×10^{-11} cm^3 molecule^{-1} s^{-1} at room temperature. The temperature dependence for this abstraction rate coefficient is well fit by the expression 1.76×10^{-11} $(T/298\ \mathrm{K})^{1.51}$ $\exp(99\ \mathrm{K}/T)$ cm^3 molecule^{-1} s^{-1} for T = 200−2000 K.

The barrier height of 0.25 kcal/mol for this TST calculation of the triplet abstraction rate coefficient was obtained at the CCSD(T)/CBS//CCSD(T)/cc-pVQZ level (from CCSD(T)/cc-pV5Z and CCSD(T)/cc-pV6Z calculations) and included corrections for higher excitations (−0.25 kcal/mol from CCSDTQ(P)/cc-pVDZ and CCSDT(Q)/cc-pVTZ results) and for core−valence correlation (0.04 kcal/mol from CCSD(T)/CBS estimates based on cc-pCVTZ and cc-pCVQZ results). The vibrational frequencies were obtained at the CCSD(T)/aug-cc-pVTZ level. The CCSDT(Q) and CCSDTQ(P) calculations employed the MRCC module of Kallay.[29,30]

The present prediction for the overall rate coefficient at room temperature is 8.5×10^{-11} cm^3 molecule^{-1} s^{-1}, with 30% of this coming from the triplet abstraction channel. This prediction is in good agreement with the experimental measurement of 11×10^{-11} cm^3 molecule^{-1} s^{-1} and is well within the combined theoretical and experimental uncertainties. At room temperature, this prediction for the triplet abstraction rate coefficient is uncertain by a factor of ∼2−3, due to uncertainties in the barrier height (∼0.5 kcal/mol) and in the lowest frequency bending mode (roughly, a factor of 1.5). In contrast, the uncertainties in our capture rate predictions are much smaller, perhaps as small as 20%, due to the basis set and active space effects discussed above, with some additional uncertainty due to the extent of any dynamical effects arising from the spin−orbit interaction.

The predicted rate coefficient k_{SO} is largely independent of temperature, as seen in Figure 4. At temperatures above 400 K, the present theoretical predictions are in fair agreement with the previous ones of Wang et al.[14] In contrast, the present result differs markedly from the previous prediction of Wang et al.[14] (reproduced in Figure 4b) for the capture rate coefficient at low temperatures, with the latter showing a significant increase in the rate coefficient at temperatures below 400 K. (Note that, in discussing the results of Wang et al.,[14] we consider only their MRCI//CASSCF predictions, since CCSD(T) calculations for radical−radical interactions at long-range are known to be inaccurate.) It is interesting to consider further the source of the discrepancy between the predicted temperature dependence of the VRC-TST method and the previous theoretical result for the association reaction. We identify three significant differences

between the present theoretical approach and the one employed in ref 14, as discussed next.

First, the present calculations employ an interaction potential obtained at the CASPT2/aug-cc-pVDZ level of theory, whereas, in the previous theoretical study, the Davidson-corrected multireference configuration interaction (CAS+1+2+Q or MRCI+Q) method with the aug-cc-pVTZ basis set was used. We previously observed that the CASPT2 and CAS+1+2+Q methods give similar results for barrierless association reactions,[7,31] and it is not clear which method may be considered more accurate in general. Although CAS+1+2+Q may be considered more theoretically rigorous, CASPT2 is size extensive, which may be important for characterizing transition states at large fragment separations. We have verified that the CAS+1+2+Q/aug-cc-pVTZ and CASPT2/aug-cc-pVDZ methods predict similar energetics along the mininum energy path for association for the present system; the CAS+1+2+Q surface is actually 10−15% *less* attractive than the CASPT2 surface for R_{CF} = 3−4.6 Å, which should yield a lower rather than higher rate coefficient.

The second significant difference between the present treatment and that of ref 14 is in the treatment of the number of states for the transition state. In ref 14, the rigid rotor/harmonic oscillator (RRHO) approximation was used. In the present VRC-TST calculations, the RRHO approximation was used for the internal degrees of freedom of CH_3, but the number of states associated with the transitional degrees of freedom was evaluated classically and with full anharmonicity and mode couplings.

To more directly compare these approximations, we carried out RRHO calculations along the minimum energy path for association at the CASPT2/aug-cc-pVDZ level of theory, which is the same level of theory used to evaluate the interaction potential in the present VRC-TST calculations. Spin−orbit splitting was neglected in the computation of the harmonic frequencies, but was included in the relative energies of the transition state species. Transition state dividing surfaces with C−X separations of 2−5 Å were included in the RRHO calculations, and the results were verified to be converged with respect to these limits. The resulting microcanonical RRHO rate coefficient is in excellent agreement with the VRC-TST result for 300−2500 K, as shown in Figure 4b. The present RRHO calculation does not show the significant negative temperature dependence reported in ref 14.

The third and final difference between the two theoretical treatments is the range of dividing surfaces considered. The RRHO calculations reported in ref 14 were variationally optimized at the microcanonical level, but the range of transition state dividing surfaces considered in the variational optimization was determined from CVT calculations. Specifically, transition state dividing surfaces with R_{CF} = 2.8−3.0 Å were considered in ref 14. In the present calculation, the CVT dividing surfaces in the RRHO calculation occurred for R_{CF} = 3−3.7 Å for 300−2500 K. Microcanonically optimized RRHO and VRC-TST rate coefficients were obtained for sets of dividing surfaces restricted to 3−3.7 Å, and, in both cases, the rate coefficient is significantly increased at temperatures below ∼600 K, as seen in Figure 4b. These results suggest that the temperature dependence reported in ref 14 is an artifact of this restriction of dividing surfaces.

The excellent agreement between the present RRHO and VRC-TST predictions is perhaps surprising. Although the predicted thermal rate coefficients are very similar, the methods differ significantly in the dynamical details of their predictions. In Figure 6, the reactive flux N is plotted along the reaction coordinate R_{CF} for several total energies and for 5$\hbar$ total angular momentum for the RRHO and VRC-TST methods. The RRHO and VRC-TST methods predict qualitatively different fluxes along the reaction coordinate, with the VRC-TST fluxes showing less dependence on fragment separation for large values of R_{CF}. There are significant differences in the fluxes predicted by the two methods at short fragment distances as well.

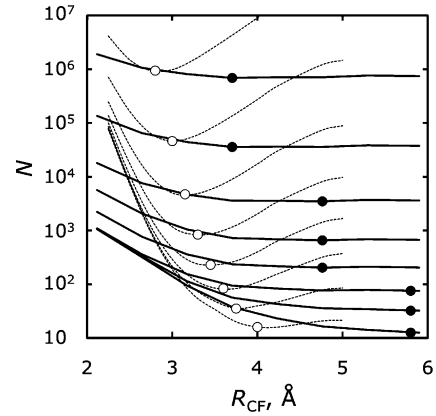

Figure 6. VRC-TST (solid) and RRHO (dotted) microcanonical fluxes for 5$\hbar$ total angular momentum and for several total energies E along the minimum energy path for CH_3 + F association. The lowest curves of each type are for E = 100 cm^{-1}, and the other curves in each series correspond to twice the total energy of the curves below them. The highest energy curve of each type is for E = 12800 cm^{-1}. The circles denote the approximate variational minima for each curve, i.e., $k(E,J = 5\hbar)$. The ordinate axis is logarithmic.

We may interpret the curves in Figure 6 as follows. The harmonic frequencies associated with the two bound transitional modes vary from 473 cm^{-1} at R_{CF} = 2.5 Å to only 27 cm^{-1} at R_{CF} = 5 Å. One may question the appropriateness of the HO approximation for such low frequency modes, which are typically highly anharmonic. In Figure 6, the RRHO method is seen to predict significantly higher fluxes than the VRC-TST method at long fragment separations, which suggests a failure of the RRHO method for these low frequency modes.

At short separations, the geometry of the CH_3 fragment begins to distort from its isolated structure. The frequency of the CH_3 umbrella motion is unperturbed from its isolated value (547 cm^{-1}) for distances larger than ∼3.5 Å and is increased to 974 cm^{-1} at R_{CF} = 2.5 Å. The frequencies associated with the remaining CH_3 internal degrees of freedom are largely unchanged over this region of the minimum energy path for association. Fragment distortion has two typically opposite effects on the flux: the frequencies of the conserved modes increase relative to their asymptotic values (which decreases the flux) and the interaction becomes more attractive (which increases the flux). Fragment distortion is included in the RRHO calculations but is neglected in the present implementation of VRC-TST. Figure 6 suggests that the VRC-TST method may underestimate the flux at short separations, as compared with the RRHO result.

The errors in the fluxes identified above affect the predicted thermal rate coefficients only if these errors change the value of the variationally optimized fluxes. Remarkably, the variationally optimized fluxes (i.e., the minima in the curves shown in Figure 6) have similar values for the RRHO and VRC-TST methods (although the RRHO values are 10−40% larger than the VRC-TST ones for the curves shown in Figure 6), despite occurring at significantly different fragment separations. The variationally optimized RRHO fluxes occur at shorter bond separations than those for the VRC-TST method. This tendency

is reflected in the range of CVT dividing surface separations: 3.2−4.5 Å for VRC-TST and 3−3.7 Å for RRHO. The resulting RRHO and VRC-TST microcanonically optimized thermal rate coefficients are therefore found to be similar, despite these significant dynamical differences.

The qualitative trends appearing in Figure 6 may be expected to be general, although the near numerical equivalence of the minima in the fluxes is unlikely. The dynamical differences between the RRHO and VRC-TST methods have important consequences in the present context of spin−orbit coupled systems. Specifically, the magnitude of the spin−orbit splitting may be significantly different at the RRHO and VRC-TST dividing surfaces, which may influence the predicted kinetics. We have already shown that spin−orbit splitting has a minor effect on the VRC-TST rate coefficient for the CH_3 + F reaction, but these dynamical differences may have more important kinetic implications for other spin−orbit coupled systems.

Product branching in the CH_3 + F reaction and CH_3F dissociation was previously characterized in detail theoretically.[14] The present revision of the capture rate coefficient could have an effect on the predicted rate coefficients, especially at low temperatures. A full characterization of the CH_3 + F reaction is beyond the scope of the present work.

CH_3 + Cl. The VRC-TST capture rate coefficient for the CH_3 + Cl association reaction is $7-10 \times 10^{-11}$ cm^3 molecule^{-1} s^{-1} for 300−2500 K. The basis set and active space sensitivity of the predicted rate coefficient are expected to be minor, as discussed in detail for the CH_3 + F reaction, and are not considered here. When spin−orbit splitting is neglected, the VRC-TST prediction for the rate coefficient is increased by 10−13% over this temperature range.

The magnitude of this effect is similar to that observed for the CH_3 + F reaction, despite the larger spin−orbit splitting associated with Cl. Although the CH_3Cl complex is less strongly bound than the CH_3F complex, at long-range the minimum energy path for the CH_3 + Cl case is more attractive than for the CH_3 + F case (cf. Figure 2). Thus, the CVT transition state dividing surfaces for the CH_3 + Cl reaction occur at larger C−X separations than for the CH_3 + F reaction, as show in Figure 1. As a result, over the kinetically important region of the potential energy surface (R^*_{CVT} = 4.0−5.3 Å) Δ is only 20−28%, similar to that for the CH_3 + F reaction (cf. Figure 3). Again, the effect of spin−orbit splitting on the rate coefficient is roughly 1/2 the energetic perturbation Δ.

The accuracy of the *a posteri* corrections in eqs 2 and 3 is qualitatively similar to the accuracy of these corrections for the CH_3 + F reaction. Due to the larger atomic spin−orbit splitting, the simple approximation in eq 2 is even less accurate for the CH_3 + Cl reaction than for the CH_3 + F reaction at low temperatures, with an error at room temperature of 70%. The error associated with the use of eqs 3 and 5 is only ∼7%, which is somewhat less than the error due to neglecting spin−orbit effects entirely.

The CH_3 + Cl capture rate coefficient was previously calculated[2] using VRC-TST and the CAS+1+2+Q/aug-cc-pVTZ potential energy surface. In the previous work, a more approximate treatment of the spin−orbit splitting was employed. The spin−orbit splitting was assumed to be a one-dimensional step function of R_{CCl} centered at 4 Å. The results were observed to be very sensitive to the choice of the center of the step function. In Figure 1, we see that for a wide temperature range 1300−2500 K, the canonical dynamical bottleneck occurs at ∼4 Å, which explains the observed sensitivity. The present calculations are in good agreement with the previous calculation at low and high temperatures, although the two methods predict somewhat different temperature dependences. The present explicit treatment of the spin−orbit splitting is expected to be more accurate. We note that the present improvement of the CH_3 + Cl capture rate coefficient does not significantly affect the accuracy of the predicted low pressure limit rate coefficients presented and compared with experimental measurements in ref 2.

CH_3 + Br. The VRC-TST capture rate coefficient for the CH_3 + Br reaction is $0.9-1.3 \times 10^{-10}$ cm^3 molecule^{-1} s^{-1} for 300−2500 K. If spin−orbit splitting is neglected, the predicted rate coefficient is increased by only 5−10%. Although the spin−orbit splitting associated with the Br atom is significant, R^*_{CVT} = 3.7−5.3 Å for 300−2500 K, and the spin−orbit splitting deviates relatively little from its asymptotic value over this kinetically important region of the potential energy surface. Specifically, Δ for R_{CBr} = 3.7−5.3 is ∼27−34% (cf. Figure 3). This small deviation is again related to the increased long-range attractiveness and correspondingly larger transition state separations. The more gradual change in ε_{SO} as a function of R_{CBr} (cf. Figure 1) also contributes the smallness of Δ.

The use of eq 2 to correct k^c_{SO} results in major errors at low temperatures; at 300 K, the rate is underestimated by eq 2 by a factor of 200. The corrected rate obtained using eqs 3 and 5 is only 10% lower than k_{SO}, which is similar to the error associated with neglecting the geometry dependence of spin−orbit splitting entirely.

The rate coefficient for the CH_3 + Br → CH_3Br reaction was previously measured[15] relative to that for methyl recombination at room temperature and from 1−100 bar He. The extrapolated high pressure limiting rate coefficient obtained in that study ($1.19 \pm 0.25 \times 10^{-10}$ cm^3 molecule^{-1} s^{-1}) is 36% larger than the present value (8.75×10^{-11} cm^3 molecule^{-1} s^{-1}), which is just within the combined experimental and theoretical uncertainties.

Closer agreement between the present theory and previous experiment is obtained by considering the pressure dependence of the CH_3 + Br → CH_3Br reaction. Preliminary master equation simulations demonstrate that the finite pressure data from ref 15 may be reproduced accurately using the present theoretical capture rate. We note that the present reinterpretation of the experimental results avoids the unusual pressure dependence suggested by the original analysis, as pointed out elsewhere.[2]

Finally, we note that the CH_3 + Br rate coefficient was measured relative to that of CH_3 + CH_3, which was assumed in ref 15 to have the high pressure limiting value of 6.5×10^{-11} cm^3 molecule^{-1} s^{-1}. A recent VRC-TST calculation[8] predicts this rate to be ∼30% lower (4.6×10^{-11} cm^3 molecule^{-1} s^{-1}), which may indicate a corresponding adjustment to the rate for CH_3 + Br. The ratio of the VRC-TST rate coefficients for CH_3 + Br and CH_3 + CH_3 at 300 K (1.8) is in agreement with the measured value of Kransoperov et al. (1.65 ± 0.26 at 100 bar).

III.C. Allyl Radical−Halogen Atom Reactions. *CH_2CHCH_2 + F.* The VRC-TST capture rate coefficient for the CH_2CHCH_2 + F reaction is $7-9 \times 10^{-11}$ cm^3 molecule^{-1} s^{-1} for 300−2500 K. The rate for F addition to allyl radical is ∼20% faster than the rate for F addition to CH_3, indicating that the steric hindrance of the bulkier allyl radical is offset by the availability of the two reactive carbons and the stronger dispersion interactions. The CVT dividing surfaces for the allyl reaction occur at R^*_{CVT} = 2.8−3.8 Å, and these separations are 0.4−0.7 Å shorter than R^*_{CVT} for the CH_3 + F reaction. This observation is consistent with the shorter-ranged transition states identified previously for the reactions of resonantly stabilized radicals with H atoms relative to H atom addition to other radicals.[9]

If the geometry dependence of the spin−orbit splitting is neglected, the predicted rate coefficient is increased by only ∼5% for 300−2500 K, which is somewhat less than Δ = 7−20% for R^*_{CVT} = 2.8−3.8 Å. Although Δ is not predictive of the quantitative effect on the rate coefficient (it is generally too high), Δ correctly predicts the trend that the effect of spin−orbit splitting will be less significant for the allyl reaction than for the methyl reaction.

The use of eqs 2 and 3 results in relative errors very similar to those discussed above for the CH_3 + F reaction. Again, eq 2 introduces considerable error at low temperatures, and the error associated with eq 3, which is only ∼10%, is similar to the error introduced by assuming a geometry-independent spin−orbit splitting.

CH_2CHCH_2 + Cl. The VRC-TST capture rate coefficient for the CH_2CHCH_2 + Cl reaction is 9−10 × 10^{-11} cm^3 $molecule^{-1}$ s^{-1} for 300−2500 K, which is very close to the rate for Cl addition to CH_3. If the geometry dependence of the spin−orbit splitting is neglected, the predicted rate coefficient is increased by only ∼5% for 300−2500 K. The value of Δ for this system is 4−20% for R^*_{CVT} = 3.2−5.2 Å. The error from the use of eq 2 is 70% at room temperature and decreases with increasing temperature, and the error associated with eqs 3 and 5 is ∼10%. The accuracy of these simple models for the allyl + Cl reaction is very similar to that for the CH_3 + Cl reaction.

CH_2CHCH_2 + Br. The VRC-TST capture rate coefficient for the CH_2CHCH_2 + Br reaction is 5−7 × 10^{-11} cm^3 $molecule^{-1}$ s^{-1}, and, at high temperatures, the rate is a factor of 2 lower than the rate for Br addition to CH_3. The CVT dividing surfaces for 300−2500 K show an abrupt change in the dynamical bottleneck around 500 K, as shown in Figure 1. At higher temperatures, the CVT dividing surfaces for the CH_2CHCH_2 + Br reaction occur at significantly shorter fragment separations than those observed in the CH_3 + Br reaction.

If the geometry dependence of the spin−orbit splitting is neglected, the predicted rate coefficient is increased by 37−102% for 300−2500 K, which is significantly greater than the effect observed for the other reactions considered here. This result cannot be explained by Δ, which for this system is only 17−24% for R^*_{CVT} = 3.2−6.7 Å and is similar in magnitude to the other reactions.

The use of the simple correction in eq 2 leads to significant errors, especially at low and moderate temperatures, as observed for the CH_3 + Br reaction. Equation 3 is more accurate, but the error remains significant (∼40%) up to 500 K. We conclude that the perturbative corrections in eqs 2 and 3 are not enough to explain the significant effect that the geometry dependence of the spin−orbit splitting has on the predicted rate coefficients for this reaction, particularly at low temperatures.

As shown in Figure 1, the CVT dividing surfaces for the k_{SO} and k^c_{SO} calculations differ significantly from one another for the CH_2CHCH_2 + Br reaction, with R^*_{CVT} differing by 0.5−1.5 Å for 500−2000 K. This is in contrast to the other reactions considered here, where R^*_{CVT} values were very similar for the two sets of calculations. Apparently, the increased steric interactions and the asymptotically large spin−orbit interaction (with a corresponding possibility for a large reduction at short range) combine to make a sharp transition to a short transition state separation of about 3 Å for this allyl + Br case. We conclude that the explicit consideration of the geometry dependence of the spin−orbit splitting qualitatively changes the shape of the CH_2CHCH_2 + Br potential energy surface in the dynamically relevant region, giving rise to a nonperturbative change in the predicted kinetics. This nonperturbative change is not well described by the simple models in eqs 2 and 3, and a full dynamical treatment is required.

Bedjanian et al.[16] determined the room temperature rate for CH_2CHCH_2 + Br addition in their study of the reactions of Br with propene. Their value of 2.0 ± 0.5 × 10^{-10} cm^3 $molecule^{-1}$ s^{-1} is a factor of 3 larger than the present theoretical value. We note that the experimental study assumed a rate for allyl recombination of 1.1 × 10^{-11} cm^3 $molecule^{-1}$ s^{-1}, and experimental[32] and recent theoretical[10] determinations of the rate for allyl recombination are roughly 3 times larger. The use of a lower rate for allyl recombination may have resulted in increased rates for allyl + Br, although their analysis shows their results to be insensitive to the self-recombination rate. Finally, we note that dynamical spin−orbit coupling (i.e., electronic transitions due to spin−orbit coupling), which is neglected here, may be significant for this reaction.

III.D. Trends in the Alkyl Radical−Halogen Atom Association Kinetics. The rate coefficients for halogen addition to CH_3 and CH_2CHCH_2 are typically of similar magnitude despite the significantly different nature of the hydrocarbon radicals. This trend may also be observed in the VRC-TST predictions for rates for H addition to CH_3 and CH_2CHCH_2,[7,9] which differ from one another by less than 15%. The increased steric repulsion of the bulky allyl fragment is largely offset by the presence of two reactive carbon atoms instead of one and the increased dispersion interactions. Br addition is the exception, where the rate for addition to the allyl radical is a factor of 2 less than that for addition to methyl. This difference is apparent only when the geometry dependence of the spin−orbit splitting is explicitly considered, as discussed above. If the geometry dependence of the spin−orbit splitting is neglected, the rates for Br addition to allyl and methyl differ by less than 5%.

Halogen atom addition is 3−6 times slower than H atom addition for both the methyl and allyl radicals. The rates for the CH_3 + X reactions are similar in magnitude to the CH_3 + OH addition rate,[3] with similarly minor temperature dependence. No significant trends emerge in the hydrocarbon radical−halogen atom addition rates with respect to the three halogen atoms considered here. The rates for Cl addition to CH_3 and CH_2CHCH_2 are 20−50% faster than those for F addition. Br addition is faster than F addition for CH_3 but is slower than F addition for CH_2CHCH_2.

IV. Conclusions

VRC-TST rate coefficients were calculated for the CH_3 + X and CH_2CHCH_2 + X (X = F, Cl, and Br) association reactions. The energetic role of spin−orbit splitting on the predicted rate coefficients was considered in detail. The region of the potential energy surface where the spin−orbit coupling varies most strongly was shown to occur over the same range of fragment separations where the important dynamical bottlenecks for association occur.

For each system, two sets of rate calculations were performed. In one, the geometry dependence of the spin−orbit splitting was explicitly considered, and, in the other, the spin−orbit splitting was assumed to be constant and equal to the spin−orbit splitting of the isolated halogen atom. The neglect of the geometry dependence of the spin−orbit splitting systematically increased the predicted rate coefficient but the effect was *typically* a minor one (5−15%) and was roughly 1/2 of the relative change in the interaction energy near the dynamical bottlenecks for association. This effect is small, but it may be expected to be somewhat larger than errors in the calculation associated with the use of finite basis sets and limited active spaces.

The minor effect of spin−orbit splitting on the calculated rate was rationalized in terms of a modified Boltzmann-weighted energetic correction (eq 3), and such a simple model provided good results for five of the six reactions so long as the energetic correction was determined at the variational transition states and a temperature-dependent energy splitting less than the atomic splitting was used. The error associated with eq 3, however, was found to be similar to that obtained by neglecting spin−orbit effects entirely (∼10%).

The other limiting assumption of zero spin−orbit splitting in the transition state region (eq 2) yields much larger errors and should generally be avoided for radical−radical reactions.

The allyl + Br reaction was not well described by the simple perturbative model. The effect of explicitly calculating the spin−orbit splitting was significant, decreasing the rate coefficient by as much as a factor of 2. The dynamical bottlenecks for the allyl + Br reaction occur over a large range of fragments separations and were found to be significantly shifted toward shorter fragment separations by the spin−orbit splitting. We concluded that the kinetic effect of spin−orbit splitting on the allyl + Br rate was therefore not perturbative, with a full treatment of the geometry dependent spin−orbit splitting required for accurate results.

The treatment of the CH_3 + F barrierless transition state was considered in detail. The thermal rate coefficient predicted by the RRHO method was shown to agree well with the VRC-TST rate coefficient, as long as dividing surfaces at sufficiently large fragment separations were included in the microcanonical variational optimizations. The two methods predicted significantly different dynamical details, however. At the large fragment separations associated with low temperature (below ∼500 K) dynamical bottlenecks, the presence of low frequency modes (∼20 to 100 cm^{-1}) in the transition state species caused the RRHO method to greatly overestimate the density of states. At the shorter fragment separations associated with the high temperature dynamical bottleneck, the absence of geometry relaxation caused the VRC-TST method to underestimate the flux. These tendencies caused the RRHO method to predict CVT dividing surfaces over a much narrower and shorter range of fragment separations than predicted by the VRC-TST method. These differences could have important implications for kinetics calculations involving geometry dependent properties such as spin−orbit splitting, although a significant difference in the thermal rate coefficient for the RRHO and VRC-TST methods was not observed here for the CH_3 + F reaction.

In this work, we considered the energetic effect that the spin−orbit splitting associated with halogen atoms has on the hydrocarbon radical-halogen atom association kinetics. We did not consider the dynamical effect of spin−orbit coupling, and the present analysis assumes that the association reactions occur exclusively on the ground state potential energy surface. In future work we will consider the dynamical effect of spin−orbit coupling on hydrocarbon radical-halogen atom association rate coefficients using non-Born−Oppenheimer molecular dynamics.[33] Dynamical effects may be particularly important for Br and Cl.

Acknowledgment. The authors would like to thank Yuri Georgievskii for many helpful interactions. This work is supported by the Division of Chemical Sciences, Geosciences, and Biosciences, Office of Basic Energy Sciences, U.S. Department of Energy. The work at Argonne was supported by contract number DE-AC02-06CH11357. Sandia is a multiprogram laboratory operated by Sandia Corporation, a Lockheed Martin Company, for the United States Department of Energy under Contract No. DE-AC04-94-AL85000.

References and Notes

(1) Tashiro, M.; Schinke, R. *J. Chem. Phys.* **2003**, *119*, 10186.
(2) Parker, J. K.; Payne, W. A.; Cody, R. J.; Nesbitt, F. L.; Stief, L. J.; Klippenstein, S. J.; Harding, L. B. *J. Phys. Chem. A* **2007**, *111*, 1015.
(3) Jasper, A. W.; Klippenstein, S. J.; Harding, L. B.; Ruscic, B. *J. Phys. Chem. A* **2007**, *111*, 3932.
(4) Klippenstein, S. J. *J. Chem. Phys.* **1992**, *96*, 367.
(5) Klippenstein, S. J. *J. Phys. Chem.* **1994**, *98*, 11459.
(6) Georgievskii, Y.; Klippenstein, S. J. *J. Chem. Phys.* **2003**, *118*, 5442.
(7) Harding, L. B.; Georgievskii, Y.; Klippenstein, S. J. *J. Phys. Chem. A* **2005**, *109*, 4646.
(8) Klippenstein, S. J.; Georgievskii, Y.; Harding, L. B. *Phys. Chem. Chem. Phys.* **2006**, *8*, 1133.
(9) Harding, L. B.; Klippenstein, S. J.; Georgievskii, Y. *J. Phys. Chem.* **2007**, *111*, 3789.
(10) Georgievskii, Y.; Miller, J. A.; Klippenstein, S. J. *Phys. Chem. Chem. Phys.* **2007**, *9*, 4259.
(11) Jasper, A. W.; Klippenstein, S. J.; Harding, L. B. *J. Phys. Chem. A* **2007**, *111*, 8699.
(12) World Meteorological Organization, Scientific Assessment of Ozone Depletion, 2006; Global Ozone Research and Monitoring Project Report 50, 2007.
(13) Beiderhase, T.; Hack, W.; Hoyermann, K. *Z. Phys. Chem.* **1995**, *188*, 227.
(14) Wang, L.; Kislov, V. V.; Mebel, A. M.; Yang, X.; Wang, X. *Chem. Phys. Lett.* **2005**, *406*, 06.
(15) Krasnoperov, L. V.; Mehta, K. *J. Phys. Chem. A* **1999**, *103*, 8008.
(16) Bedjanian, Y.; Poulet, G.; Le Bras, G. *J. Phys. Chem. A* **1998**, *102*, 5867.
(17) Georgievskii, Y.; Harding, L. B.; Klippenstein, S. J.; *VaReCoF*; Sandia National Laboratories and Argonne National Laboratory: Argonne, IL, 2006.
(18) Georgievskii, Y.; Klippenstein, S. J. *J. Phys. Chem. A* **2003**, *107*, 9776.
(19) Andersson, K.; Malmqvist, P.-A.; Roos, B. O. *J. Chem. Phys.* **1992**, *96*, 1218. Werner, H.-J. *Mol. Phys.* **1996**, *89*, 645. Celani, P.; Werner, H.-J. *J. Chem. Phys.* **2000**, *112*, 5546.
(20) Dunning, T. H., Jr. *J. Chem. Phys.* **1989**, *90*, 1007.
(21) Kendall, R. A.; Dunning, Jr., T. H.; Harrison, R. J. *J. Chem. Phys.* **1992**, *96*, 6796.
(22) Peterson, K. A.; Figgen, D.; Goll, E.; Stoll, H.; Dolg, M. *J. Chem. Phys.* **2003**, *119*, 11113.
(23) DelBene, J. E. *J. Phys. Chem.* **1993**, *97*, 107.
(24) Berning, A.; Schweizer, M.; Werner, H.-J.; Knowles, P. J.; Palmier, P. *Mol. Phys.* **2000**, *98*, 1823.
(25) Moore, C. E. *Atomic Energy Levels*; NSRDS-NBS 35; Office of Standard Reference Data, National Bureau of Standards: Washington, DC, 1971.
(26) Nicklass, A.; Peterson, K. A.; Berning, A.; Werner, H.-J.; Knowles, P. J. *J. Chem. Phys.* **2000**, *112*, 5642. Berning, A.; Schweizer, M.; Werner, H.-J.; Knowles, P. J.; Palmieri, P. *Mol. Phys.* **2000**, *98*, 1823.
(27) Slater, J. C. *J. Chem. Phys.* **1964**, *41*, 3199.
(28) Martin, J. M. L.; Uzan, O. *Chem. Phys. Lett.* **1998**, *282*, 16.
(29) MRCC, a string-based quantum chemical program suite written by M. Kállay. See also Kállay, M.; Surján, P. R. *J. Chem. Phys.* **2001**, *115*, 2945. as well as: www.mrcc.hu.
(30) Kállay, M.; Gauss, J. *J. Chem. Phys.* **2005**, *123*, 214105.
(31) Harding, L. B.; Klippenstein, S. J.; Jasper, A. W. *Phys. Chem. Chem. Phys.* **2007**, *9*, 4055.
(32) Jenkin, M. E.; Murrells, T. P.; Shalliker, S. J.; Hayman, G. D. *J. Chem. Soc. Faraday Trans.* **1993**, *89*, 433.
(33) Jasper, A. W.; Nangia, S.; Zhu, C.; Truhlar, D. G. *Acc. Chem. Res.* **2006**, *39*, 101.

JP1015092